J Sign Process Syst (2014) 74:263–271
DOI 10.1007/s11265-013-0796-5

Signal Processing and Application of Six-axis Force/Torque Sensor Integrated in Humanoid Robot Foot

Baoyuan Wu · Qingquan Yan · Jianfei Luo · Zhongcheng Wu

Received: 26 March 2013 / Accepted: 31 May 2013 / Published online: 8 June 2013

Abstract Six-axis force/torque sensor (*F*/*T* sensor) that can detect three orthogonal forces and torques has been extensively adopted in humanoid robot foot for stable control. Due to the F/T sensors being seriously influenced by the electromagnetic interference from ankle generator, signal stability of *F*/*T* sensor is still one of the main influencing factors for accurately dynamical and stable control. Though the problem with influencing electromagnetic noise can be solved generally and partially by shielding of the sensor and wires, this traditional method will to some extend face implementation difficulty induced by special mounting space and application environment especially in humanoid robot ankle. Therefore, the research on the output signal stability and precision of the *F*/*T* sensors has still been one of the most essential subjects for humanoid robot dynamic equilibrium control. In this paper, some various signal processing methods have been adopted and analyzed comparatively with the aim at the output signal anti-interference processing of F/T sensors. And the filtering effect and its feasibility were verified experimentally in the dynamic walking motion of humanoid robot platform BHR-2.

Keywords Signal Processing · FIR Filtering · Six-axis Force/Torque Sensor · Humanoid Robot

B. Wu (✉) · Q. Yan
Institute of Intelligent Machines, Chinese Academy of Sciences, Hefei 230031, China
e-mail: bywu@iim.ac.cn

Q. Yan
e-mail: qqyan@ustc.edu.cn

J. Luo · Z. Wu
High Magnetic Field Laboratory, Chinese Academy of Science, Hefei 230031, China

J. Luo
e-mail: jfluo@ustc.edu.cn

Z. Wu
e-mail: zcwu@iim.ac.cn

1 Introduction

The realization of dynamic and stable walking anthropomorphically for humanoid robots to step on various kinds of uneven environments, has long been considered as the research emphases in the field of humanoid robot. The foot system constitutes the element which ensures the interaction between the humanoid robot and the environment [1–6].

At present, six-axis force/torque sensor (*F*/*T* sensor) has also been extensively used in humanoid robot foot for external force detection along with the dynamic equilibrium criterion (*ZMP*) [7–10] for stable control. For stable and dynamic walking gait, it is a very important achievement to obtain precisely the real-time forces and moments acted on the foot and to use those intelligently to generate appropriate motions planning by using adequate control algorithms. To get better stability and dynamic walking gait of humanoid robots, *F*/*T* sensor integrated in humanoid robot foot (*at the level of ankle*) along with the *ZMP* criterion and diverse control schemes, have been widely adopted for the realization of humanoid robots such as ASIMO [11], HUBO [12], HRP-2 [13, 14], WIBIAN-III [15], and BHR-2 [16], etc. to walk stably and dynamically in human living space.

The concept of the *ZMP* is useful for understanding dynamic stability and also for monitoring and controlling a robot walking, which needs external forces and torques (contact forces and other forces due to gravity and inertial effect) to be detected real-timely [16–20]. For accurate measurement of three forces and three torques in humanoid robot foot, the six-axis *F*/*T* sensor should be designed and fabricated in consideration of robot's weight and the height of foot. The adopted *F*/*T* sensor has also played an important role and deemed one of the most important performances for the objective of fast and stable walking anthropomorphically of robot [21, 22]. However, the output signal stability of *F*/*T* sensor is still one of the main influencing factors for accurately dynamical and stable control of humanoid robot.

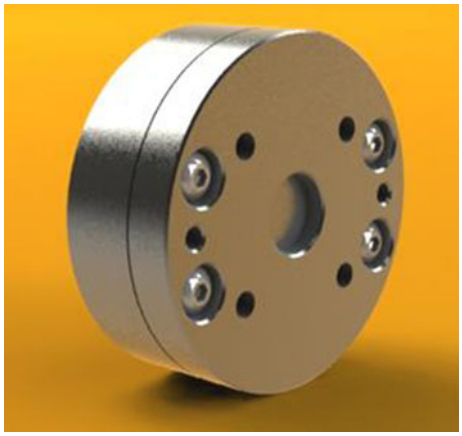

Figure 1 Photograph of the self-made *F*/*T* sensor.

Because the *F*/*T* sensors are usually set at the level of robot ankle, and the output signal are seriously influenced by the electromagnetic interference from the ankle generator/motor. Though the problem with influencing electromagnetic noise can be solved generally and partially by shielding of the sensor and wires, this traditional method will to some extend face implementation difficulty induced by special mounting space and application environment especially in humanoid robot ankle. Therefore, the research on the output signal stability and precision of the *F*/*T* sensors has still been one of the most essential subjects for humanoid robot dynamic equilibrium control.

In this paper, we will mainly concern ourselves with the aim at the output signal anti-interference processing of the F/T sensors. Firstly, the general overview of the *F*/*T* sensor is given in section 2. Secondly, some various signal processing methods are proposed respectively and characteristic test on

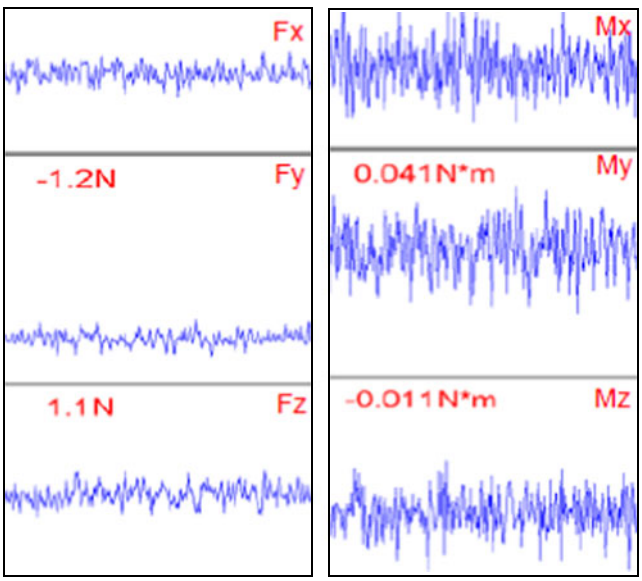

Figure 2 Primitive output of the F/T sensor.

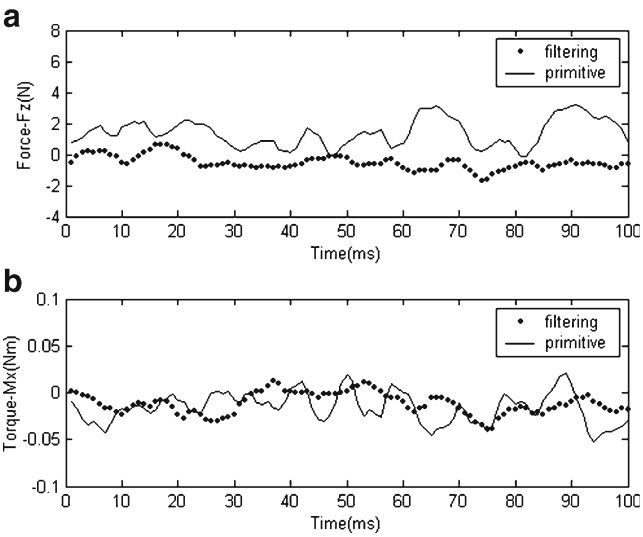

Figure 3 Comparison of filtering output by SMF and the primitive output in (**a**) Force-F_z and (**b**) Torque-M_X.

F/*T* sensor in section 3. Finally, the experiments on signal stability of *F*/*T* sensor mounted in the integrated perceptual foot(IPF) system of humanoid robot BHR-2 have been conducted and some conclusions are reached in section 4 and section 5.

2 Overview of the *F*/*T* Sensor

The *F*/*T* sensor integrated in humanoid robot foot should withstand the impact of loading and measure three forces F_X (x-direction force), F_Y, F_Z and three torques M_X (x-direction torque), M_Y, M_Z for dynamic equilibrium control. The applied forces and torques are detected via the *F*/*T* sensor mounted to the level of robot ankle. The self-developed *F*/*T*

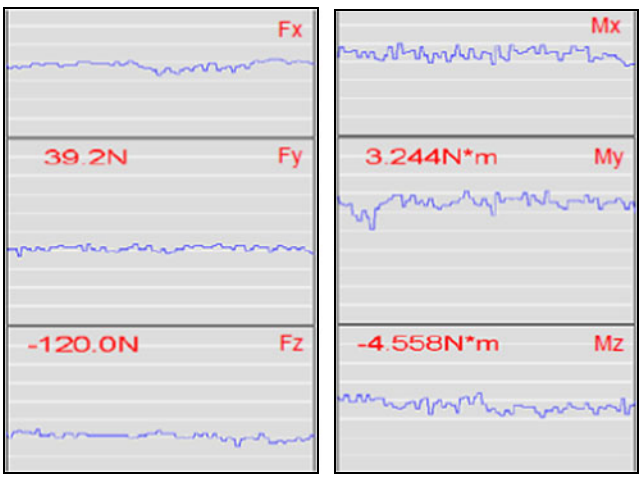

Figure 4 Comparison of filtering output by MF & SMF and the primitive output in Forces (*left column*) and Torques (*right column*).

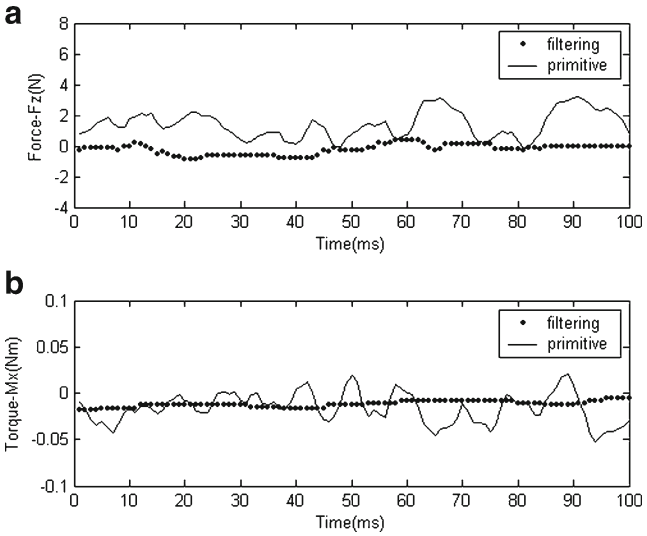

Figure 5 Comparison of filtering output by STF and the primitive output in (**a**) Force- F_Z and (**b**) Torque-M_X.

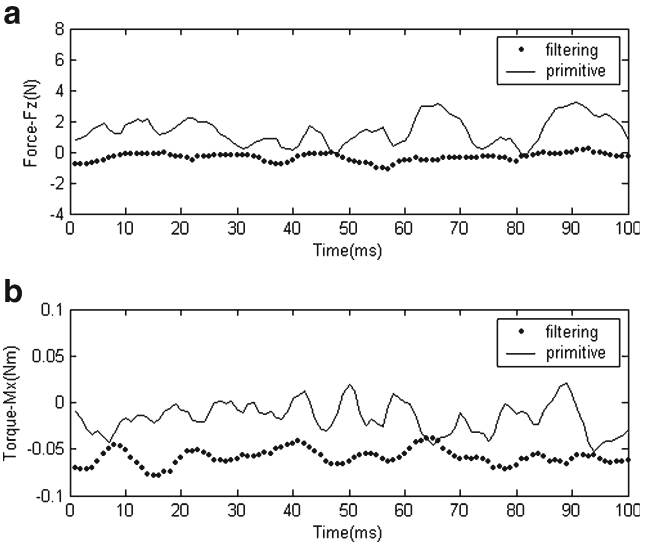

Figure 7 Comparison of filtering output by DTF and the primitive output in (**a**) force-F_Z and (**b**) Torque-M_X.

sensor is 67 mm*25.5 mm (diameter*height) in dimension and weighs 370 g. (as shown in Fig. 1)

The *F*/*T* sensor developed in this paper can measure three torques up to 50 Nm along the roll axes, pitch axes and yaw axes and three normal forces up to 800 N in the X, Y direction, and 1500 N in Z direction. Moreover, we can calculate X, Y position of *ZMP* in X-Y plane. It consists of six-full strain gage bridges attached to the mechanical structure of sensor to measure three torques and three forces. The calibration test is achieved by applying many different load cases. The sensor includes an overload mechanical protection and it can bear a total impact force nearly up to 2400 N.

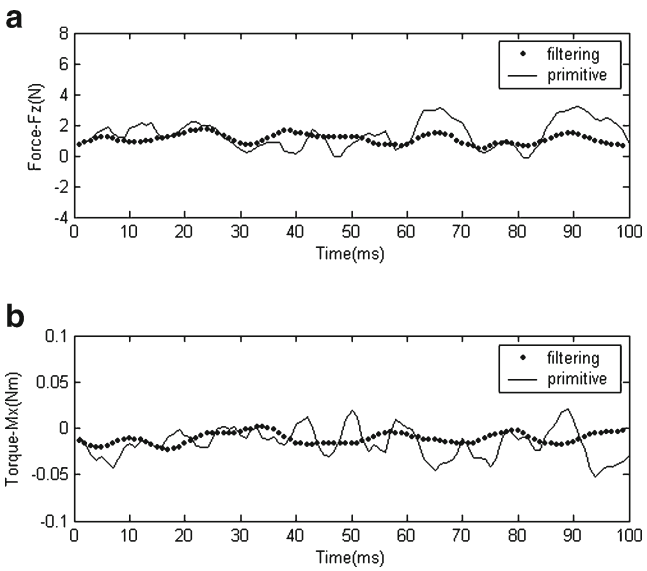

Figure 6 Comparison of filtering output by STF & SMF and the primitive output in (**a**) Force-F_Z and (**b**) Torque-M_X.

3 Signal Processing of the *F*/*T* Sensor

3.1 Effect Comparison of Different Signal Processing Methods

Before choosing filtering method, it is necessary to observe the characteristic of the primitive output data of the *F*/*T* sensor for designing a suitable filtering method. Figure 2 provides the primitive output data (without any filtering) of the *F*/*T* sensor. Obviously, the primitive wave of output data is interfered seriously by the noise with great data fluctuation and many outstanding burrs and spikes.

Commonly, we first take the sliding mean filtering (SMF) into consideration because this method can smooth output wave simply and is convenient to calculate. Namely a sampled values x_i (i = 1,2,..,N, where N is the length of the formation) are regarded as a formation in succession. Put the new sampled datum x_{n+1} at the tail of the formation and simultaneously throw away the datum x_1 each time. Then carry on arithmetic average operation of these data in this formation, the filtering result can be obtained by

$$y\left(y = \left(\sum_{i=2}^{N+1} x_i\right)\Big/ N\right) \tag{1}$$

Take the force F_Z and torque M_X for example, Fig. 3 provides the output wave of the *F*/*T* sensor after the sliding window filtering while the result is still relatively undesirable. Researching the cause that the mean filtering is being sensitive to pulses and the frequent burr exerts a tremendous influence to the mean value.

For the characteristics of the output data of *F*/*T* sensor being interfered seriously by pulses, median filtering (MF) and SMF

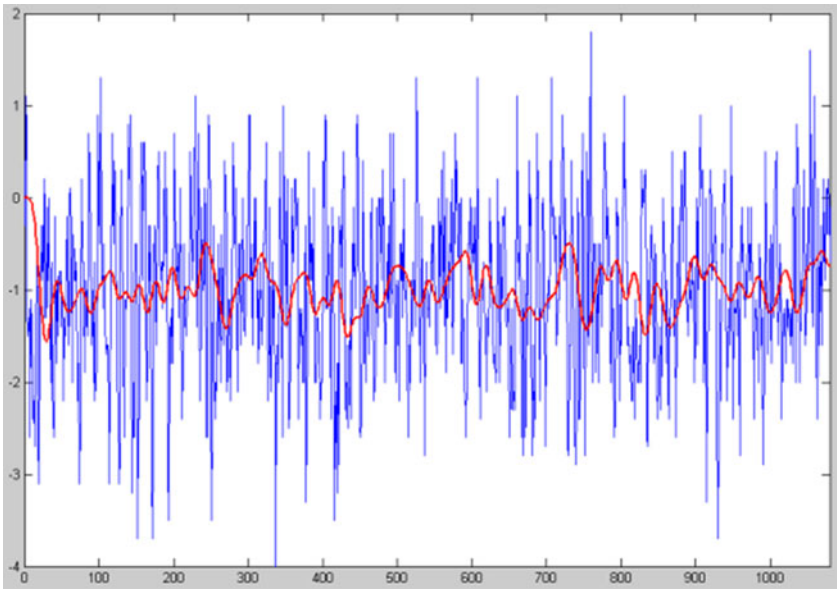

Figure 8 Comparison of filtering output by FIR and the primitive output in force-F_Z.

are surely adopted to dispel the sharp burrs successively. Figure 4 provides a filtering result obtained by this method. However, the output data F/T sensor is a six dimensional feature vector, the application of mean filtering has still been confronted many thorny problems.

Comparatively, the ideal situation is: within any period, the output values of the F/T sensor fluctuate in a narrow range around the average value of n data. Therefore the single-threshold filtering (STF) has been adopted with the main thought: a) Fetch the average value of n data as the reference datum X_a; b) gather the current data xi to compare with the mean value; c) if the difference value $\Delta = |x_i - X_a|$ is greater than the threshold value (Sth) set in advance, namely, $\Delta >$ Sth, consider xi as an interfering data and the mean value being set as the present output; d) otherwise consider xi an effective data. Figure 5 shows the outputs still have frequent spikes after single-threshold filtering.

In view of the deficiency of STF, it may be improved by the adoption of combination of STF and SMF. And the experimental results are shown in Fig. 6.

However, there are defects of adding the new element into sliding window by using STF method. Though the difference between the primitive data and mean value is greater than the threshold value, it will still need to move the primitive data into sliding window for the calculation of mean value in the next step. Thus it is still more sensitive to pulses, so the data will drift with time after filtering. If abandon primitive data completely, namely it will lead to decrease the real-time performance of the F/T sensor.

As for elimination of interference while in unloading states and tracking the dynamic course of the F/T sensor while in loading states, the dual-threshold filtering (DTF) method has been adopted with the main principle: set the limit of threshold value and compare with the difference value between the primitive value and the mean value in sliding window. And then, judge whether the primitive output is effective or not.

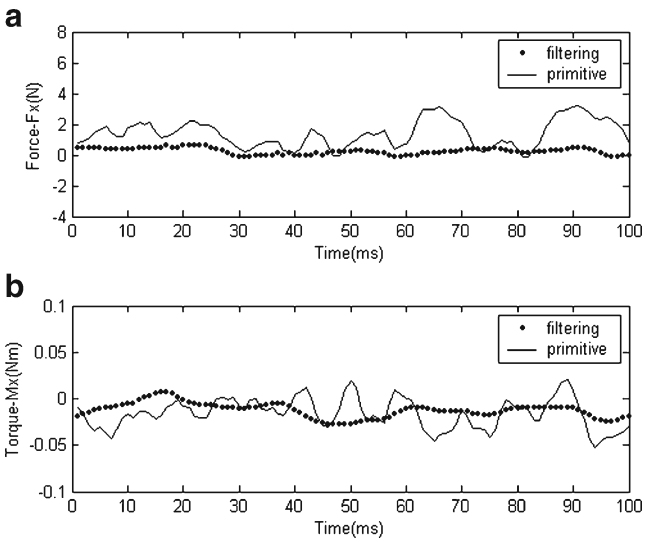

Figure 9 Comparison of filtering output by DTF & FIR and the primitive output in (**a**) force-F_Z and (**b**) Torque-M_X.

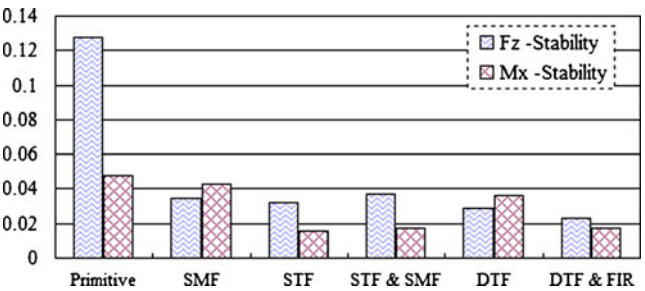

Figure 10 Stability (λ) comparison of every filtering method.

Table 1 Rated output of simulation analysis and characteristic test of the *F*/*T* sensor.

F/*T* sensor	Rated output (mV/V)		
	Simulation	Experiment	Error (%)
F_X	0.288	0.283	1.87
F_Y	0.288	0.292	−1.25
F_Z	0.288	0.301	−4.37
M_X	0.824	0.842	−2.18
M_Y	0.824	0.780	5.34
M_Z	0.628	0.602	4.19

Specifically, if $S_{Low\_th} \le S_{diff} \le S_{Upp\_th}$, then consider the primitive output as an interfering data and the mean value will be set as the present output. Where S_{Low_th} and S_{Upp_th} are the lower limit and the upper limit of threshold value, respectively. Where, $S_{diff} = |S_{primitive} - S_{mean\_slid}|$ is the difference value between the primitive output $S_{primitive}$ and the mean value in sliding window S_{mean_slid}. If $S_{diff} \ge S_{Upp\_th}$ or $S_{diff} \le S_{Low\_th}$, then consider $S_{primitive}$ as an effective value and mean that the *F*/*T* sensor is in loading states or the primitive output is in the fluctuation range allowed. Figure 7 shows the results after DTF.

Though the results obtained from the above several methods have certain effects, it still can not reach the anticipated goal. The output of *F*/*T* sensor is interfered by high frequency with burrs present frequently. So the low pass filter is comparatively the best choice first in next consideration with combination of the method above for better effect of filtering.

Finite impulse response (FIR) is a low pass filtering with characteristics of the linear phase with mathematical expression defined by

$$y[n] = x[n]*h[n] = \sum_{i=0}^{N} x[i]h[n-i] \tag{2}$$

Where $x[n]$ is the sampled input sequences, $y[n]$ is the filtering output. Certainly, we design a FIR low pass filter with 31 steppes (achieved by utilizing the software: MATLAB), the filtering effect of the primitive output is more remarkable.

According to the filtering coefficient obtained through MATLAB, realization of the FIR low pass filtering algorithm has been achieved experimentally via DSP processor. Figure 8 shows the filtering results of force F_Z.

As can be seen from that above, we notice that it eliminate the interference of high frequency with the waveform output comparatively smooth through FIR low pass filtering. Nevertheless, the amplitude of fluctuating is still partially large, so a new thought is taken into consideration by using the combination of DTF and FIR low pass filtering method. The filtering results are shown in Fig. 9.

In order to comparatively evaluate the filtering methods mentioned above, here the evaluation index of stability λ is defined by

$$\lambda = \frac{MAX(\Delta_i|V_i - W_i|)}{F_s} \times 100\%, \quad i = 1, 2, \ldots, N \tag{3}$$

where, Vi is the output of the *F*/*T* sensor after filtering, W_i is the mean value calculated by N data of the *F*/*T* sensor. F_s is the relevant full-scale range of forces and torques. The stability results (where $N = 10$) obtained from every filtering method are listed in Fig. 10.

3.2 Characteristic Test on F/T Sensor

The characteristic test for interference error of the *F*/*T* sensor is carried out by applying rated force F_X first, the outputs of force/moment in every dimensional direction F_Y, F_Z, M_X, M_Y and M_Z are measured, respectively. The rated output based on simulation analysis can be calculated by

$$U_o = UK\varepsilon/4 \tag{4}$$

where, U_o is the output voltage of the Wheatstone bridge, K is the factor of strain-gauge (*2.06*), U is the input voltage of the Wheatstone bridge. ε is the total strain.

Table 1 shows the rated output from simulation analysis and characteristic test of force/moment in every dimensional

Table 2 The static and dynamic indexes of the developed *F*/*T* sensor.

Indexes	F_X	F_Y	F_Z	M_X	M_Y	M_Z
Sensitivity (S) (με/N, με//Nm)	0.55	0.55	0.8	80	80	24. 9
Nonlinearity (FS %)	0.06	0.05	0.06	0.37	0.22	0.75
Precision (FS %)	0.01	0.01	0.01	0.02	0.02	0.02
Stability Errors (FS%)	0.05	0.05	0.05	0.05	0.05	0.05
Non-repeatability Errors (FS%)	0.02	0.02	0.02	0.04	0.04	0.04
Natural Frequency	1815	1815	1723	2695	2695	2751
$f(x)$	21					
W	7.3					

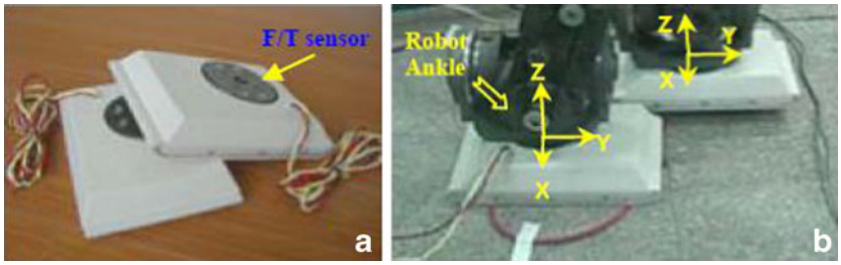

Figure 11 **a** Photo of the IPF system mounted the *F*/*T* sensors and **b** The walking experiment environment of BHR-2.

direction of the *F*/*T* sensor. The errors of the results from characteristic test based on the results from simulation analysis are also listed here.

Though the characteristic matrix represents the corresponding relationship between the output and input of *F*/*T* sensor, it can not reflect the actual output/input among channels of *F*/*T* sensor in virtue of the error effects from mechanical processing, signal conditioning, patches alignment and fabrication, etc. Thus it needs compensation and modification through quantitative analysis based on the calibration error matrix *E* which is written by

$$E = (F_S - F)F_f^{-1} \tag{5}$$

where, F_s, F are the standard loading force matrix and the force matrix calculated from the characteristic matrix, respectively. $F_f = diag(F_{fx}\ F_{fy}\ F_{fz}\ M_{fx}\ M_{fy}\ M_{fz})$ is a 6 × 6 diagonal matrix, here F_{fx}, F_{fy}, F_{fz}, M_{fx}, M_{fy}, M_{fz} are the full scale outputs of *F*/*T* sensor under the loading forces F_X, F_Y, F_Z and moments M_X, M_Y, M_Z, respectively. Those off-diagonal elements in the matrix *E* denote the coupling level among channels, which are known as interference error.

Equation (6) indicates the interference error in every dimensional direction of the developed *F*/*T* sensor. The maximum interference error for F_X is 2.13 %, for F_Y is 0.23 %, for F_Z is 0.77 %, for M_X is 1.69 %, for M_Y is 1.14 %,

$$E = \begin{bmatrix} 1 & 0.00131 & -0.00420 & 0.00444 & 0.01135 & 0.01089 \\ -0.00607 & 1 & -0.01106 & 0.00151 & -0.00517 & 0.01221 \\ 0.01653 & -0.00189 & 1 & -0.00243 & 0.00139 & -0.00607 \\ 0.00000 & -0.00231 & 0.00185 & 1 & -0.01064 & 0.00069 \\ -0.00496 & 0.00023 & 0.00767 & 0.01691 & 1 & 0.00248 \\ -0.02133 & -0.00100 & 0.00100 & -0.00367 & -0.00766 & 1 \end{bmatrix} \tag{6}$$

for M_Z is 1.22 %. The main reasons of causing interference errors generally are machining accuracy of spare part, location error of strain-gage, installing debugging, calibration, environmental conditions, precision of the instruments, etc.

Indeed, the *F*/*T* sensor with maximum interference error 2.13 % for F_X can generally meet the practical requirement of precision for robot balance control. However, with the development of humanoid robot aims to realize anthropomorphic gait like human, the *F*/*T* sensor with higher comprehensive performances is needed essentially. So the quantitative compensation and modification of interference error of the *F*/*T* sensor has been conducted on the basis of the calibration error matrix *E*, which is given by

$$C_E = (V - E + I)F_f F^{-1} \tag{7}$$

where, C_E is the modified characteristic matrix of *F*/*T* sensor. *I* is a 6 × 6 identity matrix. After compensation for characteristic matrix, interference error of the *F*/*T* sensor decreased remarkably but not to zero because of the system error of calibration set up. The precision test results indicate that the overall precision is less than 1 % shown in Table 2.

3.3 Discussion

It comparatively makes perfect result by combination of the dual-threshold filtering and FIR low pass filtering in low frequency, and the output data stability of the *F*/*T* sensor improves greatly. However, the phenomenon of zero drift is comparatively outstanding. It is analyzed that the possible reason may be caused by temperature drift of the sensor body material. So we can consider carrying on the temperature compensation while in hardware design of *F*/*T* sensor. Furthermore, the static result is better when the FIR works in a lower cutoff frequency while the dynamic response to the input with high frequency is comparatively poor. And it is surely clear that the dynamic characteristics should be emphatically considered in the structural design of *F*/*T* sensor beforehand.

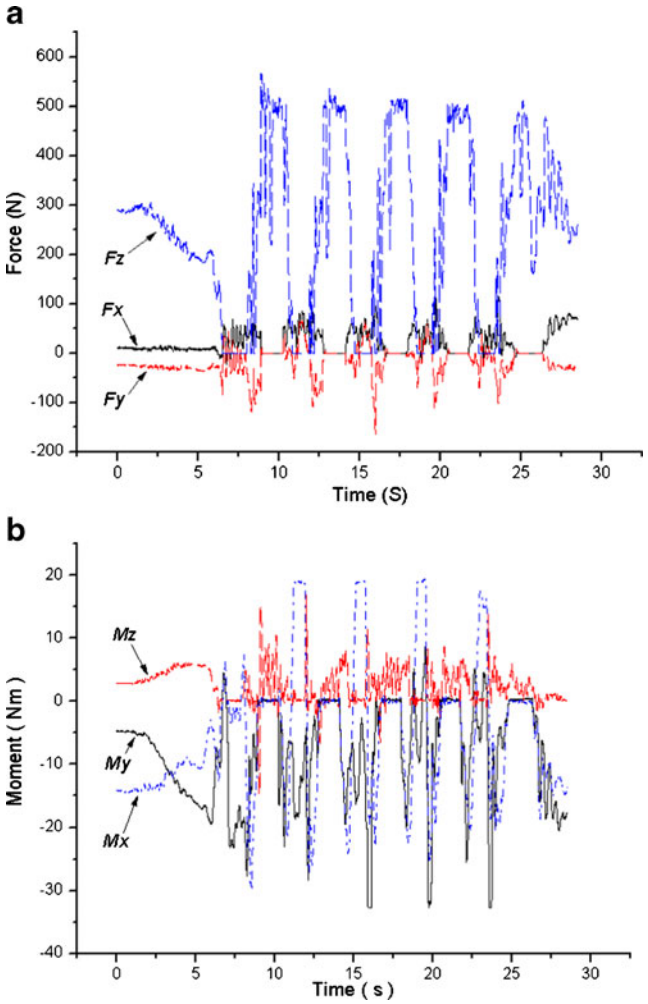

Figure 12 Evolution of (**a**) forces and (**b**) torques measured with the IPF system in robot's walking.

In addition, what else needs to be noted that it is effective by combining the methods applied above in the improvement of precision and stability. And it should be taken primarily into consideration the dynamic demands in the optimum design of *F*/*T* sensor for practical applications in specific fields.

4 Experiments

The Experimental researches on the comprehensive performances of *F*/*T* sensors are essentially important to verify the feasibility and validity for humanoid robot to keep dynamical stability in real time on unexpected ground. Indeed, some balance control schemes of humanoid robot based on the dynamic criterion *ZMP* can be achieved by means of two *F*/*T* sensors to detect real-timely the external contact forces/torques between the feet and ground. In order to obtain overall understanding of performance, the dynamically walking experiments have been conducted with two *F*/*T* sensors mounted between the IPF system and each ankle of humanoid robot BHR-2, respectively [23]. Walking experiments for the IPF system integrated in the ankle level of the humanoid robot BHR-2 have been comprehensively conducted and the experimental results of every system unit are listed respectively in the following sections.

Figure 11 shows the evolution of forces and torques acted on the foot system and Fig. 12 shows the *ZMP* trajectory of foot in single-support phase, which indicates that the *F*/*T* sensor system can real-timely acquire the external forces acted on the foot and better meet the real-time requirements for humanoid robot to maintain stable control based on forces while in dynamic walking.

Figure 13 shows the evolution of the ZMP trajectory of foot in single support phase in robot's walking. The actual *ZMP* position in single support can be calculated by Eq. 8, and the actual *ZMP* position in double support can be derived from that (X_{ZMP}, Y_{ZMP}) in single support which can be calculated by

$$\begin{cases} X_{\text{zmp}} = \dfrac{x_a m(a_z+g) - m a_x z_a + x_s F_Z - z_s F_X - M_Y}{m(a_z+g)+F_z} \\ Y_{\text{zmp}} = \dfrac{y_a m(a_z+g) - m a_y z_a + y_s F_Z - z_s F_Y - M_X}{m(a_z+g)+F_Z} \end{cases} \tag{8}$$

Where m is the mass of the component under *F*/*T* sensor. (a_x, a_y, a_z) are the acceleration of foot in the X-axis, Y-axis and Z-axis direction respectively. (x_a, y_a, z_a) is the center

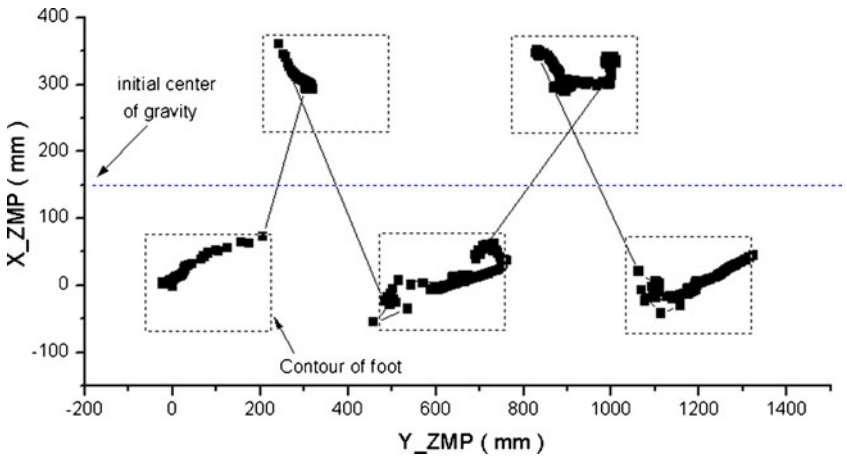

Figure 13 Evolution of the *ZMP* trajectory of foot in single-support phase in robot's walking.

position of gravity of components under the F/T sensor, (x_s, y_s, z_s) is the measurement coordinate center of the F/T sensor.

5 Conclusions and Future Works

Humanoid robots are a new and promising application area for robotics. The concept of the *ZMP* is useful for understanding dynamic stability and also for monitoring and controlling a robot walking, which needs external forces and torques (contact forces and other forces due to gravity and inertial effect) to be detected via F/T sensor real timely. In order to be commercially successful, the F/T sensor plays an important role in dynamic equilibrium control on which humanoids must have reliable biped locomotion capabilities. In this paper we focused on the aspect of the processing method of signal stability of F/T sensor system. Some signal processing schemes are contrastively adopted and analyzed to verify the feasibility of application. Experiments results indicate that FIR&DTF is more superior in stability to the others and achieves expected effect in robot walking experiments.

However, it is noticed especially that the adoption of filtering methods should be taken comprehensively into consideration the application requirements of F/T sensor. Especially in the filed of humanoid robot control, for instance, it is essentially important to weigh the signal stability and dynamic performance. And the reasonable determination of the filtering coefficient of FIR has also had an effect on practical application of the F/T sensor.

Acknowledgments 1) This work presented in this paper was financially supported by the National Project of High-Tech and Research Program ("863" project) under Grant 2008AA04Z205, and the Anhui Provincial Natural Science Foundation under Grant 1308085MF86.

2) The authors give sincere thanks to the Intelligent Robotics Institute of Beijing Institute of Technology for experiments supports.

References

1. Buschmann, T., Lohmeier, S., & Ulbrich, H. (2009). Humanoid robot lola: Design and walking control. *Physiology, 103*, 141–148.
2. Espiau, B., & Sardain, P. (2000). *The anthropomorphic biped robot BIP2000* (pp. 3996–4001). San Francisco: Proceedings of the IEEE Int. Conf. on Robotics & Automation.
3. Kim, J.-Y., Park, I.-W., & Lee, J. (2005). *System design and dynamic walking of humanoid robot KHR-2* (pp. 1431–1436). Barcelona: IEEE Int. Conf. on Robotics and Automation.
4. Konno, A., & Sellaouti, R. (2002). *Design and development of the biped prototype ROBIAN* (pp. 1384–1389). Washington: IEEE Int. Conf. on Robotics and Automation.
5. Leel, J., et al. (2006). *Development of a humanoid robot platform HUBO FX-1* (pp. 1190–1194). Korea: Int. Joint Conference on SICE-ICASE.
6. Lohmeier, S., Buschmann, T., & Ulbrich, H. (2009). *Humanoid robot LOLA* (pp. 775–780). Orlando: IEEE Int. Conf. on Robotics and Automation.
7. Kajita, S., & Kenji Kaneko, E. (2007). *ZMP-based biped running enhanced by toe springs* (pp. 3963–3969). Roma: IEEE Int. Conf. on Robotics and Automation.
8. Takubo, T., et al. (2009). *Rough terrain walking for bipedal robot by using ZMP criteria map* (pp. 788–793). Kobe: IEEE Int. Conf. on Robotics and Automation.
9. Kurt, O., & Erbatur, K. (2006). *Biped robot reference generation with natural ZMP trajectories* (pp. 403–410). Turkey: IEEE AMC'06-Istanbul.
10. Vukobratovic, M., & Stepanenko, J. (1972). On the stability of anthropomorphic systems. *Mathematical Biosciences, 15*, 1–37.
11. Hirose, M., & Ogawa, K. (2007). Honda humanoid robots development. *Phil. Trans. R. Soc. A, 365*, 11–19.
12. Hirohisa, H., Fumio, K., & Kenji, K. (2004). Humanoid robotics platforms developed in HRP. *Robotics and Autonomous Systems, 48*, 165–175.
13. Pfeiffer, F., Loffler, K., & Gienger, M. (2002). *The concept of jogging JOHNNIE* (pp. 3129–3135). Washington: Proc. of the 2002 I.E. International Conference on Robotics & Automation.
14. Tellez, R., Ferro, F., & Garcia, S. (2008). *Reem-B: An autonomous lightweight human-size humanoid robot* (pp. 462–468). Korea: 2008 8th IEEE-RAS International Conference on Humanoid Robots.
15. Kaneko, K., Kanehiro, F., & Kajita, S. (2004). *Humanoid Robot HRP-2*. New Orleans: Proc. of the 2004 I.E. International Conference on Robotics and Automation.
16. Weimin Z., Qiang H., and Dongyong J. (2009). Mechanical design of a light weight and high stiffness humanoid arm of BHR-03. Robotics and Biomimetics (ROBIO), IEEE International Conference on Digital Object Identifier. pp.1681–1686
17. Zhibin Li, Bram Vanderborght, Nikos G. Tsagarakis, et al.; Quasi-straightened Knee Walking for the Humanoid Robot. Modeling, Simulation and Optimization of Bipedal Walking COSMOS 18, 2013, p.117-130
18. Kim, D. W., Kim, N.-H., & Park, G.-T. (2012). ZMP based neural network inspired humanoid robot control. *Nonlinear Dynamics, 67*, 793–806.
19. Muscolo, G. G., Recchiuto, C. T., Hashimoto, K., et al. (2012). Towards an improvement of the SABIAN humanoid robot: From design to optimization. *Mechanical Engineering and Automation, 2*(4), 80–84.
20. Sheng, B., Huaqing, M., Zhongjie, Z., et al. (2012). Walking control method of humanoid robot based on FSR sensors and inverted pendulum model. *Advances in Autonomous Robotics, 7429*, 402–413.
21. Ill Woo, P., Baek Kyu, C., & Jung Yup, K. (2013). A real-time center of gravity trajectory generation of a biped humanoid under variable reference ZMP trajectory. *Applied Mechanics and Materials, 284-287*, 1734–1738.
22. Hashimoto, K., Asano, T., & Yoshimura, Y. (2013). Overload protection mechanism for 6-axis force/torque sensor, romansy 19 – robot design. *Dynamics and Control, 544*, 383–390.
23. Baoyuan, W., Fei, S., Yang, R., et al. (2012). Development of an integrated perceptual foot system for humanoid robots. *Robotics and Automation, 27*(2), 217–228.

Baoyuan Wu received the B.S. degree in mechanical engineering from Shenyang Aerospace University, Shenyang, China, in 1996 and the M.S. degree in mechanical engineering from Anhui University of Science and Technology, Anhui, China, in 2007. He is currently an Associate Researcher with the Research Center for Biomimetic Sensing and Control, Hefei Institute of Intelligent Machines, Chinese Academy of Sciences, Hefei, where he received his PhD degree in 2012.

His primary research interests comprise information acquisition of multi-axis force/Torque sensors and its application in Aerospace, robot, rehabilitation engineering, etc.; human-machine system and intelligent robot perception system. He is a member of Intelligent Robot Professional Committee, Chinese Artificial Intelligence Society, and holds more than 20 invention patents.

Yan Qingquan born in 1982, received the Ph.D. degree in Control science and Engineering in 2008 from the University of Science and Technology of China. Now working at Hefei Institutes of Physical Science, Chinese Academy of Sciences as Associate Researcher. His current research area is extreme environment intelligent robot control system and machine vision in industrial application.

Jianfei Luo received the B.S degree in communication engineering from AnHui University, HeFei, China in 2007, and Ph.D. degree in mechanics engineering from University of Science and Technology of China, HeFei. Since 2012, he has been employed as a assistant researcher in the High Magnetic Field Laboratory, Chinese Academy of Sciences.

He is currently with the PIC Lab, Chinese Academy of Sciences, Hefei, Anhui, China. His research interests include design of embedded systems, human-computer interface and distributed control in sensor networks.

Zhongcheng Wu received his degrees of B.A., M.A. from the Instrument Department of the Hefei Poly-Technical University of China in 1990 and 1995 respectively, Ph.D. from Chinese Academy of Science in 2001. He is the founder of HCI (Human-Computer-Interaction) Laboratory which is on pen interface, signature verification and authentication, machine sensing and biped robot gait etc. He is also a member of CHMFST (the Center of High Magnetic Field Science and Technology) on Central Controlling System for SHMFF. His Research Interests include: DCS(Distributed Controlling System), Embedded System, Networked Sensor, Pen Computing and Pen Interface, Signature Verification and Authorization.